Geophys. J. Int. (2000) **142,** 889–897

Using geomagnetic secular variation to separate remanent and induced sources of the crustal magnetic field

Vincent Lesur and David Gubbins

School of Earth Sciences, Leeds University, Leeds, LS2 9JT, *UK. E-mail: v.lesur@earth.leeds.ac.uk*

Accepted 2000 April 6. Received 2000 April 6; in original form 1999 November 16

SUMMARY

Magnetic fields originating from magnetized crustal rocks dominate the geomagnetic spectrum at wavelengths of 0.1–100 km. It is not known whether the magnetization is predominantly induced or remanent, and static surveys cannot discriminate between the two. Long-running magnetic observatories offer a chance, in principle, of separating the two sources because secular variation leads to a change in the main inducing field, which in turn causes a change in the induced part of the short-wavelength crustal field. We first argue that the induced crustal field, $\mathbf{b}^{\mathrm{I}}(t)$, is linearly related to the local core field, $\mathbf{B}(t)$, through a symmetric, trace-free matrix $\mathbf{A}$: $\mathbf{b}^{\mathrm{I}}(t) = \mathbf{A}\mathbf{B}(t)$. We then subtract a core field model from the observatory annual means and invert the residuals for three components of the remanent field, $\mathbf{b}^{\mathrm{R}}(t)$, and the five independent elements of $\mathbf{A}$. Applying the method to 20 European observatories, all of which have recorded for more than 50 years, shows that the most difficult task is to distinguish $\mathbf{b}^{\mathrm{R}}$ from the steady part of $\mathbf{b}^{\mathrm{I}}$. However, for nine observatories a time-dependent induced field fits the data better than a steady remanent field at the 99 per cent confidence level, suggesting the presence of a significant induced component to the magnetization.

Key words: crustal magnetization, induced magnetization, remanent magnetization.

1 INTRODUCTION

Magnetic prospecting is one of the most cost-effective geophysical exploration techniques. It relies on the assumption that the short-wavelength part of the geomagnetic field arises from variations in susceptibility and remanent magnetization of neighbouring crustal rocks. The observed crustal magnetic field can be used to locate and characterize the geometry of the source of magnetization. Measurements on rock samples can help with the interpretation, useful diagnostics being the susceptibility, remanence and Koenigsberger ratio (of remanent to induced magnetization). However, the relative contributions of induced and remanent magnetization in single samples do not necessarily apply to the crustal field, which arises from large-scale variations in susceptibility and remanence. It is impossible to separate the contributions of induced and remanent components to the crustal field in a static survey, made at a single epoch of time when the inducing field remains constant, without further assumptions. Often, any magnetization parallel to the main core field is assumed to be induced and the rest remanent.

True separation of induced and remanent magnetization can only be achieved when the inducing field varies with time. Goldstein & Ward (1966) proposed and developed a method for *in situ* separation using micropulsations, natural variations in the magnetic field with periods of tens of seconds. The period is sufficiently short for effects caused by electromagnetic induction to be important. The technique has been developed more recently by Clark *et al.* (1998) using differential vector magnetometry to find the Koenigsberger ratio and direction of remanent magnetization for sources that are assumed to be confined to small volumes.

In this paper we attempt to use geomagnetic secular variation, the natural variation of the main field that takes place on a decadal timescale, measured at magnetic observatories to infer an induced component of magnetization in the underlying crust. There are two steps: first, the short-wavelength component must be isolated by subtracting the core field, and then the time dependence of all three components of the residual must be shown to be consistent with a physical distribution of susceptibility in the known core field.

Isolating the short-wavelength component of the secular variation requires a dense network of permanent observatories, with spacings of a few hundred kilometres, because only permanent observatories monitor secular variation accurately. Measuring the time variations requires long-running observatories because of the decadal timescale of the secular variation. Europe is the only place where both these conditions are met: we have found some 20 observatories that have run continuously for 50 years or more.

The layout of the paper is as follows. We first justify the use of station corrections at permanent magnetic observatories to represent the crustal field. We then show that the induced component of the crustal field may be approximated by just

five time-independent parameters, each one an integral of the susceptibility in the surrounding region. The remanent magnetization requires three further parameters. An exact solution for these eight parameters can in principle be found from just three measurements of the crustal field. At the end of Section 2 we give a practical method for solving the problem using damped least squares and many measurements of the magnetic field. In Section 3 we apply the method to long-running European magnetic observatories.

2 METHOD

2.1 Crustal corrections

Main field models are constructed from observations by assuming that the field is large scale and of internal origin. Typically the geomagnetic coefficients appearing in the spherical harmonic expansion of an internal field are fitted to the data by least squares. The series may be truncated, as in the production of IGRF main field models (Barraclough & Malin 1968), or damped to be smooth at the core–mantle boundary (Shure *et al.* 1982). Residuals from these core or main field models are attributed to fields of external and crustal origin.

Permanent geomagnetic observatories provide a continuous record of the geomagnetic field. In this paper we use annual means, which exclude short-period external field effects. If the crustal component is independent of time it will affect main field models equally at all epochs. A set of crustal corrections, one for each component of the main field, may be determined from one epoch and used to improve models for other epochs. Bloxham *et al.* (1989) computed crustal corrections from epoch 1980, which has a particularly good data set thanks to Magsat, and applied them to other epochs throughout the 20th century. However, if the crustal component is induced it will vary in time as the main field changes. Bloxham & Jackson (1992) computed time-dependent models of the main field using a combination of survey and satellite data with first time differences of observatory data. The observatories therefore controlled only the secular variation, or first time derivative of the geomagnetic field. The stationary crustal component was eliminated by the differencing. Residuals can be computed by subtracting the final model values of the main field from the data at each epoch, giving time variations attributable to external sources and the crust.

Isolating the induced component of crustal magnetization requires identification of a signal that varies rapidly in space but slowly in time, on the same timescale as the secular variation. Main field models contain an enormous number of survey and satellite data, which define the spatial scales of the main field. However, secular variation is only measured at a much smaller number of sites occupied by permanent observatories or repeat stations, and it is only possible to isolate the short wavelengths where there is a dense distribution of observatories. The separation of core (main) and crustal fields is most likely to succeed in Europe, which has a dense network of good observatories spaced a few hundred kilometres apart. They are sufficiently close to monitor small spatial wavelengths in the secular variation.

In this paper we use the station corrections of Bloxham & Jackson (1992) and restrict ourselves to European observatories. Residuals for Chambon-la-Forêt (CF3), near Paris, are shown in Fig. 1. They are typically a few tens of nanoteslas in size, with an even smaller time variation. 'Crustal corrections' computed in this way will include external fields, and some are apparent in Fig. 1 because they follow an 11-year sunspot cycle. Sabaka *et al.* (1997) solved for both internal and external fields, which reduces the external signal in the residuals somewhat, but we are still forced to attribute most of the station corrections to small spatial scales, presumably of crustal origin.

The most striking feature in Fig. 1 is the smooth time variation. What is the origin of this smooth, short-wavelength, internal signal? In this paper we explore the possibility that it arises from induced crustal fields varying in response to secular variation of the core field.

2.2 Dependence of the induced field on the core field

The crustal magnetic field $\mathbf{b}$ caused by a distribution of magnetization $\mathbf{M}(\mathbf{r})$ is given by

$$b_i(\mathbf{r}) = \frac{\mu_0}{4\pi} \int M_j(\mathbf{s}) \frac{\partial^2}{\partial r_i \partial r_j} \frac{1}{|\mathbf{r}-\mathbf{s}|} \, d^3\mathbf{s}\,, \tag{1}$$

where the integral is taken over the entire magnetized region (Blakely 1995). The crustal field caused by induced magnetization, $\mathbf{b}^{\mathrm{I}}$, is computed by replacing $\mathbf{M}$ in eq. (1) by $\chi\mathbf{B}/\mu_0$, where χ is the susceptibility (assumed isotropic throughout this paper) and $\mathbf{B}$ is the core or main field.

We assume that the crustal field is caused mainly by magnetized rocks close to the measurement point $\mathbf{r}$. This assumption is implicit in magnetic surveying but is rarely evaluated quantitatively. We make the further assumption that the induced field depends only on the magnetization within a region that is small enough for variations in $\mathbf{B}$ to be neglected, typically over distances of about 200 km. $\mathbf{B}$ can then be taken outside the integral in 1 to give

$$b_i^{\mathrm{I}} = \frac{1}{4\pi} \int \chi(\mathbf{s}) \frac{\partial^2}{\partial r_i \partial r_j} \frac{1}{|\mathbf{r}-\mathbf{s}|} \, d^3\mathbf{s} B_j\,. \tag{2}$$

The approximation is discussed fully in a companion paper by Lesur & Gubbins (in preparation).

Rewrite eq. (2) as

$$\mathbf{b}^{\mathrm{I}} = \mathbf{A}B\,, \tag{3}$$

where the elements of matrix $\mathbf{A}$ are given by

$$A_{ij} = \frac{\partial^2}{\partial r_i \partial r_j} \left[\frac{1}{4\pi} \int \chi(\mathbf{s}) \frac{1}{|\mathbf{r}-\mathbf{s}|} \, d^3\mathbf{s} \right]. \tag{4}$$

Clearly, $\mathbf{A}$ is symmetric. Its trace is

$$\sum_{k=1}^{3} A_{kk} = \nabla^2 \left[\frac{1}{4\pi} \int \chi(\mathbf{s}) \frac{1}{|\mathbf{r}-\mathbf{s}|} \, d^3\mathbf{s} \right] = \chi(\mathbf{r}) = 0\,, \tag{5}$$

which follows because ∇^2 acts on the familiar integral solution of Poisson's equation, and because $\chi(\mathbf{r}) = 0$ when the observation point is in free space. Matrix $\mathbf{A}$ therefore has zero trace. A similar result has been derived by Clark *et al.* (1998) for a point source.

2.3 Separation of remanent and induced parts

Using the approximation of the last section, the entire crustal field may be written as

$$\mathbf{b}(t) = \mathbf{A}\mathbf{B}(t) + \mathbf{b}^{\mathrm{R}}\,, \tag{6}$$

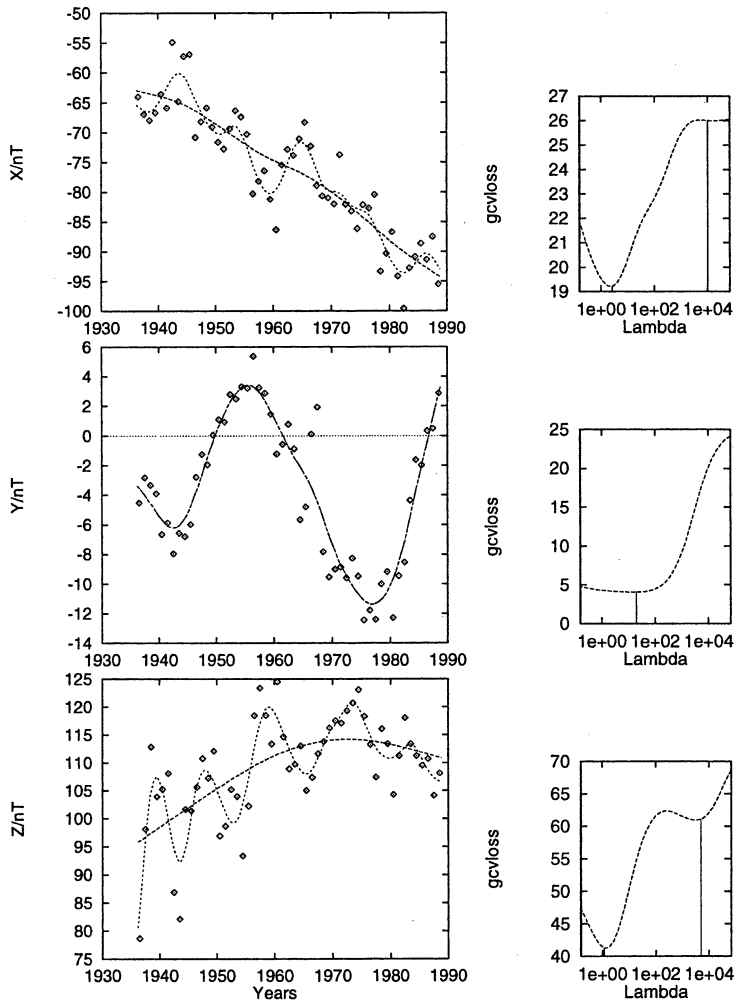

Figure 1. Chambon-la-Forêt: the left-hand figures show the crustal correction in the three components X, Y and Z (diamonds) and for each component two smooth curves that fit the data. The smoothness of these curves is controlled by a parameter λ, which is estimated by cross-validation and associated with a minimum of the GCVLOSS curves shown in the figures on the right-hand side.

where $\mathbf{b}^{\mathrm{R}}$ is the remanent component, which is independent of time. Separation of the induced and remanent parts is now a straightforward matter of inverting data for $\mathbf{b}$, the residuals at the observatories, for the five independent elements of $\mathbf{A}$ and the three components of the remanent field $\mathbf{b}^{\mathrm{R}}$. The practical method of inversion is described in the next subsection, but first it is illuminating to discuss the solution in principle.

The remanent field may be eliminated first by differentiating with respect to time:

$$\dot{\mathbf{b}}(t) = \mathbf{A}\dot{\mathbf{B}}(t)\,. \tag{7}$$

If the (time-independent) elements of $\mathbf{A}$ can be found using this equation at several different times, then $\mathbf{b}^{\mathrm{R}}$ can be found simply by substituting back into eq. (6). If $\mathbf{A}$ were a general symmetric matrix its elements could be found by applying eq. (7) at three different times. Write all three sets of equations in the form

$$\mathbf{b} = \mathbf{A}\mathbf{B}\,, \tag{8}$$

where columns of the 3×3 matrices $\mathbf{b}$ and $\mathbf{B}$ contain the components of $\dot{\mathbf{b}}$ and $\dot{\mathbf{B}}$ at the three times. The solution of eq. (8) is simply

$$\mathbf{A} = \mathbf{b}\mathbf{B}^{-1}\,, \tag{9}$$

provided $\mathbf{B}$ has an inverse, or its determinant is non-zero. In vector form the determinant reduces to the triple scalar product

$$\dot{\mathbf{B}}(t_1)\cdot\dot{\mathbf{B}}(t_2)\times\dot{\mathbf{B}}(t_3)\neq 0\,, \tag{10}$$

which is the volume of the parallelepiped given by the three vectors. Therefore, the secular variation $\dot{\mathbf{B}}$ must sweep out a finite volume for all the elements of $\mathbf{A}$ to be completely determined. In practice, we would expect more accurate determinations of $\mathbf{A}$ when secular variation has changed significantly: the main problem will be to find observatory records spanning sufficient time to encompass a large change in SV.

$\mathbf{A}$ is not a general matrix because it has zero trace and only five independent components. Its eigenvectors are orthogonal because of symmetry, and the sum of the eigenvalues is equal to the trace and therefore zero. Thus, given two eigenvectors and the corresponding eigenvalues, it is possible to construct the third eigenvector and its eigenvalue, and hence the entire matrix. This suggests that only two secular variation vectors may be needed to determine $\mathbf{A}$. The proof is illuminating and

quite simple provided one can arrange the two vectors to be orthogonal. Starting with two main field vectors $\dot{\mathbf{B}}(t_1)=\dot{\mathbf{B}}_1$ and $\dot{\mathbf{B}}(t_2)=\dot{\mathbf{B}}_2$, we construct a third vector, $\mathbf{q}$, in the same plane as $\dot{\mathbf{B}}_1$ and $\dot{\mathbf{B}}_2$ and orthogonal to $\dot{\mathbf{B}}_1$ by subtracting the projection of $\dot{\mathbf{B}}_2$ along the direction of $\dot{\mathbf{B}}_1$:

$$\mathbf{q}=\dot{\mathbf{B}}_2-(\dot{\mathbf{B}}_2\cdot\dot{\mathbf{B}}_1)\dot{\mathbf{B}}_1/|\dot{\mathbf{B}}_1|^2\,. \tag{11}$$

Now, pre-multiply by matrix $\mathbf{A}$ to give

$$\mathbf{Aq}=\mathbf{A}\dot{\mathbf{B}}_2-\frac{\dot{\mathbf{B}}_2\cdot\dot{\mathbf{B}}_1}{|\dot{\mathbf{B}}_1|^2}\,\mathbf{A}\dot{\mathbf{B}}_1=\dot{\mathbf{b}}_2-\frac{\dot{\mathbf{B}}_2\cdot\dot{\mathbf{B}}_1}{|\dot{\mathbf{B}}_1|^2}\,\dot{\mathbf{b}}_1\,, \tag{12}$$

where $\dot{\mathbf{b}}_1=\dot{\mathbf{b}}(t_1)=\mathbf{A}\dot{\mathbf{B}}_1$ from eq. (7). Everything on the right-hand side of eq. (12) is known, and therefore both $\mathbf{q}$ and $\mathbf{Aq}$ are known. We can now proceed by using the two orthogonal vectors $\dot{\mathbf{B}}_1$ and $\mathbf{q}$ instead of $\dot{\mathbf{B}}_2$.

Next, set up axes along $\dot{\mathbf{B}}_1$, $\mathbf{q}$ and $\dot{\mathbf{B}}_1\times\mathbf{q}$ so that $\dot{\mathbf{B}}_1=|\dot{B}_1|(1, 0, 0)$ and $\mathbf{q}=|\mathbf{q}|(0, 1, 0)$. The general form of matrix $\mathbf{A}$ with these axes may be taken to be

$$\mathbf{A}=\begin{pmatrix} a_{11} & a_{12} & a_{13} \\ a_{12} & a_{22} & a_{23} \\ a_{13} & a_{23} & -(a_{11}+a_{22}) \end{pmatrix}. \tag{13}$$

Substituting into eq. (7) and rearranging gives

$$\frac{\dot{\mathbf{b}}_1}{|\dot{\mathbf{B}}_1|}=\begin{pmatrix} a_{11} \\ a_{12} \\ a_{13} \end{pmatrix}, \tag{14}$$

$$\frac{\mathbf{q}}{|\mathbf{q}|}=\begin{pmatrix} a_{12} \\ a_{22} \\ a_{23} \end{pmatrix}. \tag{15}$$

This accounts for all the independent elements of $\mathbf{A}$ in eq. (13), so the matrix is found. Its elements with respect to a geographical coordinate system may be found by the usual transformation laws for rotation of axes.

The most interesting part of this proof is the construction of the vector $\mathbf{q}$. $\dot{\mathbf{B}}_1$ and $\dot{\mathbf{B}}_2$ are calculated secular variation vectors at two different times; they will be close in magnitude and direction because the historical span of measurements is short compared with the timescale of secular variation. Therefore, eqs (11) and (12) will be differences of roughly equal vectors and the result will be prone to large relative errors. This is likely to be the limiting factor in any attempt to estimate $\mathbf{A}$ from data, and we should try to find as great a change in secular variation as possible.

2.4 Inversion by least squares

In practice, equation eq. (6) poses a linear inverse problem that we solve by damped least squares. The data are the residuals at a particular observatory and the model parameters are the five independent elements of matrix $\mathbf{A}$ and the three components of remanent magnetization. These eight model parameters apply to the observatory site. Assembling the crustal corrections into a data vector $\mathbf{d}$, and the model parameters into an eight-length vector $\mathbf{m}$, eq. (6) becomes

$$\mathbf{d}(t)=\mathbf{G}(t)\mathbf{m}+\mathbf{e}\,, \tag{16}$$

where the elements of the equations of condition matrix $\mathbf{G}$ are functions of the core field $\mathbf{B}(t)$.

The data are weighted by estimating the variance on each component of the residual by its scatter about a smooth curve in time. The smooth curves were drawn by the spline cross-validation technique described by Craven & Wahba (1979); the optimal smoothness is determined by minimizing a statistic GCVLOSS that is related to the misfit between the data and the smooth curve. In our application, GCVLOSS sometimes had multiple minima and sometimes no minimum at all. Fig. 1 shows the results for the CF3 observatory. The Z-component shows two clear minima in GCVLOSS. The first minimum corresponds to the oscillatory curve that clearly follows the sunspot cycle and noise attributable to external sources. The second minimum gives the desired smooth curve describing the slow changes we wish to explain. The X-component also has two minima. Y has a single broad minimum. In cases when GCVLOSS had no minimum the smoothing was chosen by eye to produce a reasonable curve. This procedure gave rms departures of 4.64 nT in X, 1.65 nT in Y and 7.45 nT in Z for observatory CF3. Residuals in Y were usually more accurate than those in X and Z because of the smaller external signal. We assumed the errors to be independent and constructed a diagonal data covariance matrix $\mathbf{C}_e$ for each observatory.

The least-squares solution of eq. (16) was stabilized by separate damping of the remanent field and the second time derivative of the induced field. We avoided damping the first time derivative because we expected linear trends to dominate the signal from the core field. We sought the solution for $\mathbf{m}$ that minimized

$$\gamma(\mathbf{m})=\mathbf{e}^{\mathrm{T}}\mathbf{C}_e^{-1}\mathbf{e}+\theta_R^2(\mathbf{b}^R)^2+\theta_I^2\langle\ddot{\mathbf{b}}^I\rangle\,, \tag{17}$$

where the θ are damping constants and $<>$ denotes the rms time average. In matrix form this gives

$$\gamma(\mathbf{m})=(\mathbf{d}-\mathbf{Gm})^{\mathrm{T}}\mathbf{C}_e^{-1}(\mathbf{d}-\mathbf{Gm})+\theta_R^2\mathbf{m}^{\mathrm{T}}\mathbf{W}_R\mathbf{m}+\theta_I^2\mathbf{m}^{\mathrm{T}}\mathbf{W}_I\mathbf{m}\,, \tag{18}$$

where $\mathbf{W}_R$ and $\mathbf{W}_I$ are weight matrices. Minimizing eq. (18) with respect to $\mathbf{m}$ gives the usual least-squares solution

$$\mathbf{m}=(\mathbf{G}^{\mathrm{T}}\mathbf{C}_e^{-1}\mathbf{G}+\theta_R^2\mathbf{W}_R+\theta_I^2\mathbf{W}_I)^{-1}\mathbf{G}^{\mathrm{T}}\mathbf{C}_e^{-1}\mathbf{d}\,. \tag{19}$$

3 RESULTS

3.1 Effects of damping

Fig. 2 shows the effect of damping the remanent and induced fields separately. The norms $|\mathbf{b}^R|/|\mathbf{b}_0|$ and $<\ddot{\mathbf{b}}^I>/|\mathbf{b}_0|$, where $\mathbf{b}_0$ is the time average of the data (effectively the norm of the remanent component with no induced field), are plotted against the misfit to the weighted data. Zero damping gives a misfit of 1.3, on the left-hand side of the plot. In Fig. 2(a) only the remanent field is damped. The solid curve gives the remanent component, which goes to zero for extreme damping. The dashed curve gives the induced field, which follows the remanent curve downwards until a misfit of about 1.65, when it rises again.

Fig. 2(b) shows the effect of damping only the induced component. $\mathbf{b}^R$ tends to unity as the induced field approaches zero. An optimum solution is reached near misfit 1.7, where a considerable increase in norm is needed for any further improvement. Lightly damped solutions have $\mathbf{b}^R$ and $\mathbf{b}^I$ many times larger than required to explain the time-averaged residual.

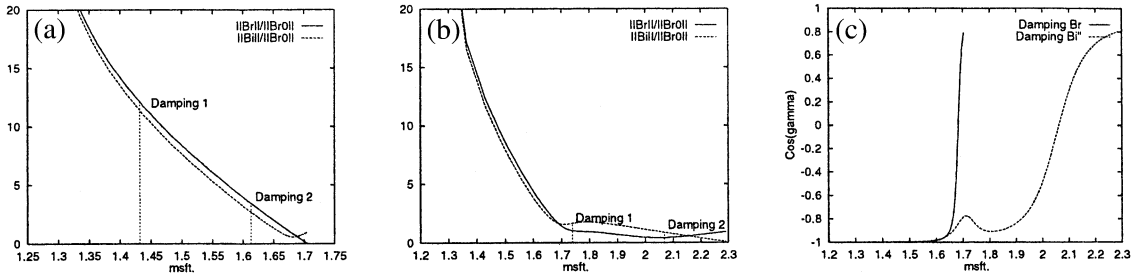

Figure 2. CF3: damping curves showing the ratio of the norm of the remanent or average induced field divided by the average of the data, as a function of the misfit. (a) Damping only the remanent field ($\theta_I = 0$ in eq. 17); (b) damping only the induced field ($\theta_R = 0$); (c) the cosine of the angle between remanent and induced components ('Damping B_R' means $\theta_I = 0$; 'Damping B_I'' means $\theta_R = 0$). 'Damping 1,2' refer to the different damping constants used to construct the corresponding curves in Fig. 3.

Fig. 2(c) gives the cosine of the angle between $\mathbf{b}^R$ and $\mathbf{b}^I$; for weak damping this is -1, indicating that the two fields are nearly antiparallel. As the damping is increased, $\mathbf{b}^R$ and $\mathbf{b}^I$ change their directions and eventually become nearly parallel at high damping, when both remanent and induced fields contribute to the average of the data.

Fig. 3 shows the fits of the model to the data for two values of the damping ['Damping 1,2' correspond to the points indicated on the damping curves in Figs 2(a) and (b)], the limit of no damping, and zero $\mathbf{b}^R$. Clearly, it is possible to fit the data reasonably well with no damping. However, we regard this solution as unphysical because it contains equal and opposite remanent and mean induced components, each over 20 times the average of the data. This is an instability in the inversion; the induced component can only fit the time variations by amplifying the average, which is balanced by the remanent component.

Physically plausible solutions lie to the right of the damping curves in Fig. 2, where the amplitudes of $\mathbf{b}^R$ and $\mathbf{b}^I$ are comparable with $\mathbf{b}_0$. For CF3 the damped solutions mainly fail to fit the time variation in Y (Fig. 3). We conclude that the core field varies too slowly to explain such oscillations, and a reasonable fit is obtained only when elements of $\mathbf{A}$ are boosted to unrealistically large values.

3.2 Comparison of long-running European observatories

20 European observatories have recorded accurately for over 50 years. They are contained within a sufficiently small region to control the core secular variation, and the residuals contain only short wavelengths not attributable to the core. The observatories are shown in Fig. 4 and details are listed in Table 1.

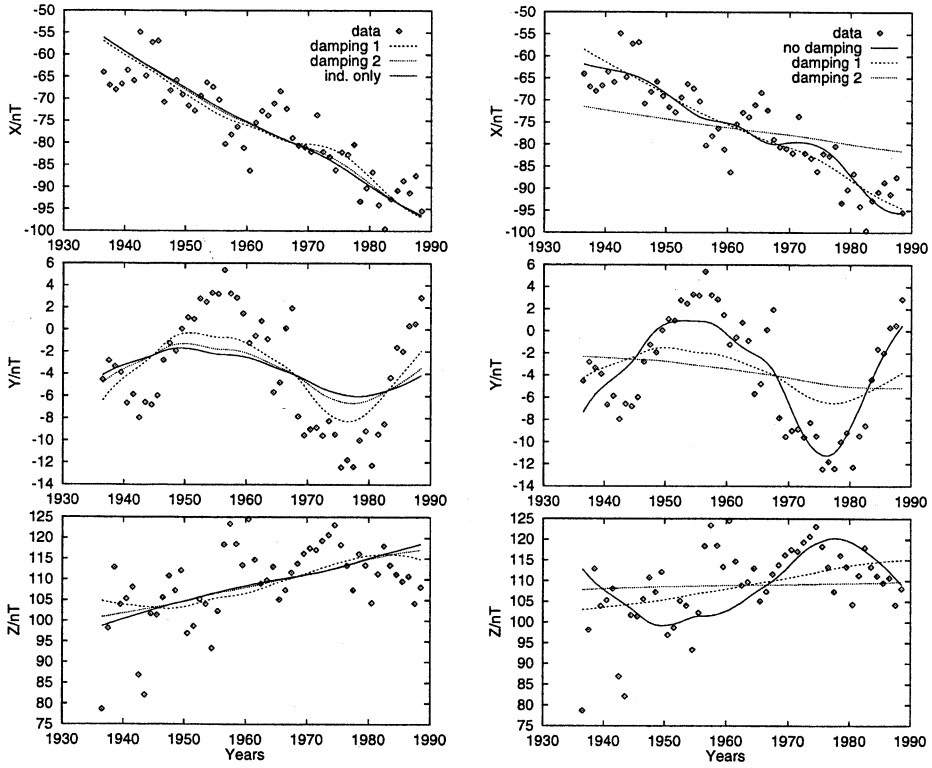

Figure 3. CF3: fit to the data when only the remanent field is damped (left) or when only the induced field is damped (right). 'Damping 1,2' correspond to the vertical lines on the graphs shown in Figs 2(a) and (b).

Figs 5–7 show the results for three of these European observatories. The signal at Lerwick in Scotland (Fig. 5) is quite different from that at CF3 (as it should be if we are to attribute it to local variations) but it produces similar problems for the inversion. At Lerwick the X-component varies significantly in time while Y has a linear trend. The model can fit Y well but not X if the solution is damped. Variations in Z are not explained by any model, mainly because of the larger error and lower weight assigned to the data (Table 1).

Fig. 6 shows results for the Niemegk observatory in Germany. The fit is excellent when the remanent field is damped but not when the induced field is damped. Again, the undamped solution contains large remanent and induced fields that are nearly equal and opposite; this is removed by damping without impairing the fit.

Fig. 7 shows data from the Lovo observatory in Sweden. Large damping is needed to obtain acceptable amplitudes of the induced and remanent fields, but no solution gives a good fit. The time variations in X and Y seem to be incompatible with the model.

3.3 A test for purely remanent or induced magnetization

Ideally we would like to determine a best-fitting solution and demonstrate that a certain combination of remanent and induced fields is required by the data, thus separating the two parts. Fig. 2(c) shows that such an attempt is futile with the data to hand. The sharp rise in the $\mathbf{b}^{\mathrm{R}}$-damped solution terminates at a misfit of about 1.7, when the remanent field is zero. Other choices of damping can only improve the misfit to about 1.6, which is not significant or justified by the increased complexity of the model.

We therefore conducted a simpler test: does a purely induced field fit the data better than a purely remanent, and therefore constant, field? A simple comparison of residuals is not sufficient to answer this question because the induced field contains five free parameters while the remanent field contains only three: other things being equal, the induced field should fit better. We tested the hypothesis by applying an F-test to compute the probability that the improvement obtained with the extra two parameters could arise at random (see e.g. Menke 1989).

The curves for a purely induced field are shown in Figs 3, 5, 6 and 7. The results from the F-test are displayed in Table 1 as a percentage. Three of the displayed observatories—Lerwick, CF3 and Niemegk—pass the test with over 99 per cent confidence: a purely induced field therefore explains the signal better than a purely remanent field, showing that at least some induced component of magnetization is required around these observatories. Lovo observatory fails the test: induced magnetization does not help to explain the time variation in the signal, and we could equally well use a constant remanent magnetization.

Table 1 gives nine observatories of the 20 that require an induced component at the 99 per cent confidence level, a further three at the 97.5 per cent level, and two more at 90 per cent. Notably, all the high-quality stations except for Lovo pass the test, and the noisier stations (judged from our criteria in the X, Y, Z columns of Table 1) fail it.

7 CONCLUSIONS AND DISCUSSION

We have shown that the induced part of the crustal magnetic field at a point can be described by five parameters related to integrals of the susceptibility, provided the signal comes from

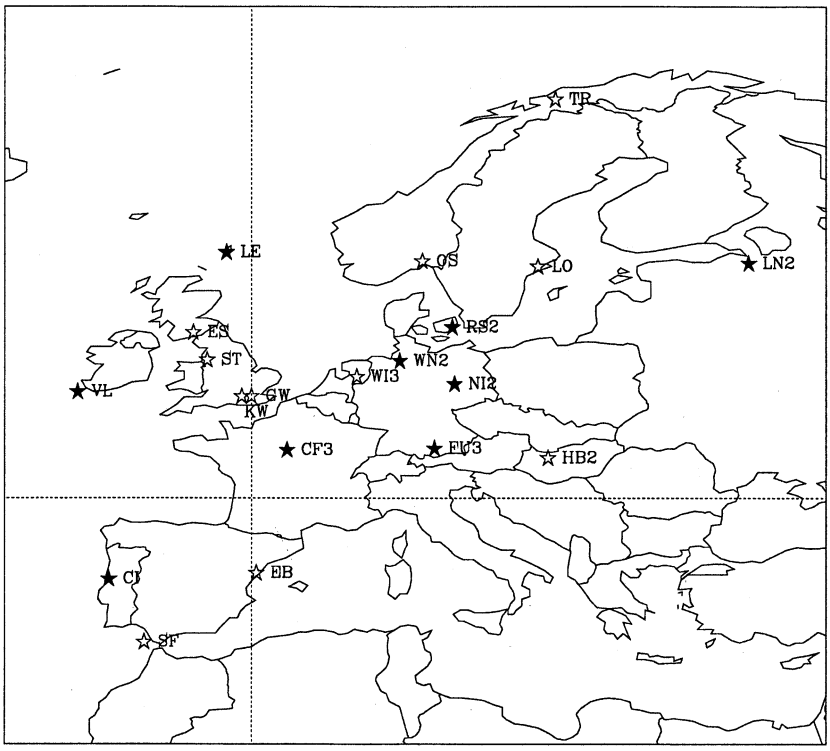

Figure 4. Map of geomagnetic observatories used in this study. Residuals at the observatories marked with a solid star require a time-dependent induced field at the 99 per cent confidence level. See also Table 1.

Table 1. Observatories used in this study. N is the number of data, SV is the largest angle between two main field vectors at different times (an indication of the magnitude of secular variation at the site), and X, Y, Z are errors estimated by fitting smooth curves. F is the confidence level that an induced field fits better than a remanent field.

Code	Name	°N	°E	Duration	N	SV°	X	Y	Z	F (per cent)
TR	Tromso	69.400	18.560	1930.5–1988.5	175	1.45	10.9	3.2	14.8	71.1
LE	Lerwick	60.080	−1.510	1923.5–1989.5	190	2.71	4.5	2.8	6.1	100.
OS	Oslo	59.550	10.430	1843.5–1930.5	234	3.54	15.8	10.6	54.1	97.6
LN2	Slutsk	59.410	30.290	1878.5–1944.5	195	2.71	4.0	4.7	12.0	100.
LO	Lovo	59.210	17.500	1928.5–1988.5	182	1.96	2.9	2.1	6.1	48.6
RS2	Rude Skov	55.510	12.270	1907.5–1980.5	222	3.33	3.7	1.8	6.6	100.
ES	Eskdalemuir	55.190	−3.520	1908.5–1989.5	245	4.08	5.2	2.7	14.0	97.6
ST	Stonyhurst	53.510	−2.680	1865.5–1943.5	226	3.98	12.6	19.6	60.6	86.6
WN2	Wingst	53.450	9.040	1939.5–1988.5	150	1.82	3.9	1.4	8.8	100.
WI3	Witteveen	52.490	6.400	1938.5–1987.5	150	1.99	4.6	2.7	6.8	94.8
NI2	Niemegk	52.040	12.410	1932.5–1988.5	171	2.26	4.2	1.7	8.5	100.
VL	Valentia	51.560	−10.550	1899.5–1989.5	273	5.04	6.7	5.9	48.7	99.6
GW	Greenwich	51.290	0.000	1846.5–1925.5	220	4.23	18.6	12.5	35.1	81.9
KW	Kew	51.280	−0.590	1857.5–1924.5	202	3.56	7.5	8.3	31.3	94.7
FU3	Furstenf.	48.100	11.170	1939.5–1988.5	150	2.10	4.7	2.1	5.7	99.6
CF3	Chambon	48.010	2.160	1936.5–1988.5	159	2.78	4.6	1.7	7.4	100.
HB2	Hurbanovo	47.520	18.110	1894.5–1986.5	174	4.54	9.8	5.5	18.6	98.8
EB	Ebro	40.490	0.300	1905.5–1980.5	202	5.69	9.5	5.7	18.1	72.6
CI	Coimbra	40.130	−8.650	1866.5–1988.5	339	9.80	13.0	8.9	31.5	100.
SF	San Fernando	36.280	−6.520	1891.5–1979.5	263	7.90	19.0	11.8	57.2	50.2

'local' rocks. Here 'local' means the region where the core field may be taken to be a constant, a typical length scale of 200 km. The result does not hold if the crustal field is dominated by very long wavelengths, but this seems unlikely. The point is discussed in full in a companion paper by Lesur & Gubbins (in preparation). The remanent part of the crustal field is described by a further three parameters.

The eight parameters may be found only if the crustal field can be separated from the core field. In practice this is done by spatial scale; again this is not possible if the crustal field is dominated by very long wavelengths. The induced part of the crustal field is isolated by differentiating with respect to time, which exacerbates the problem of core–crust separation because only the sparse network of observatories monitors the

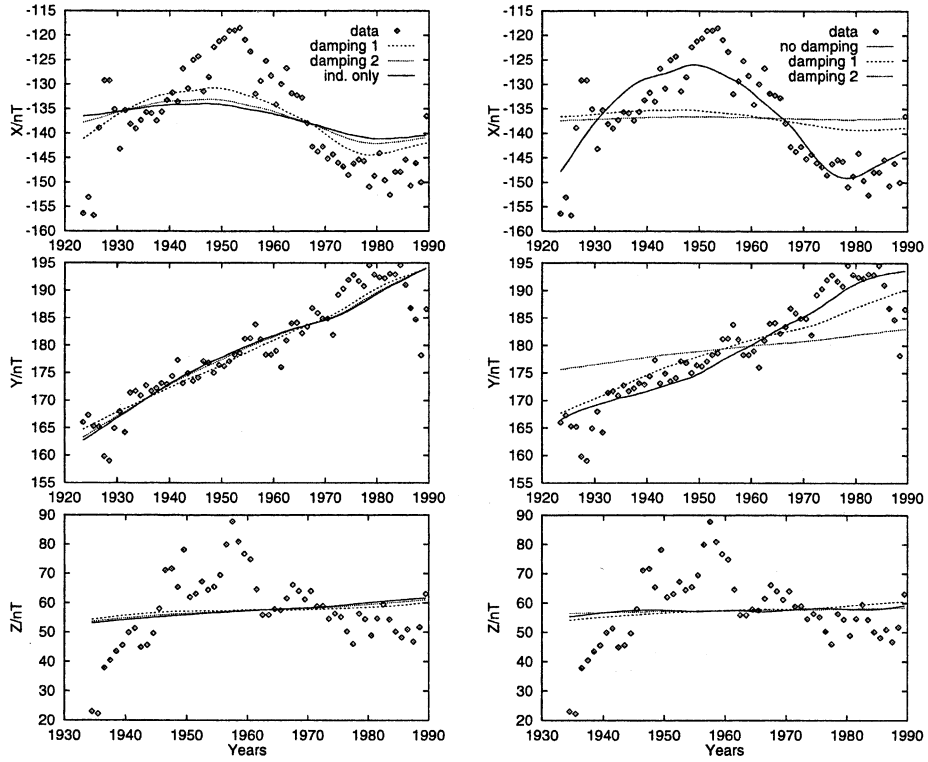

Figure 5. Lerwick: fit to the data when only the remanent field is damped (left) or when only the induced field is damped (right).

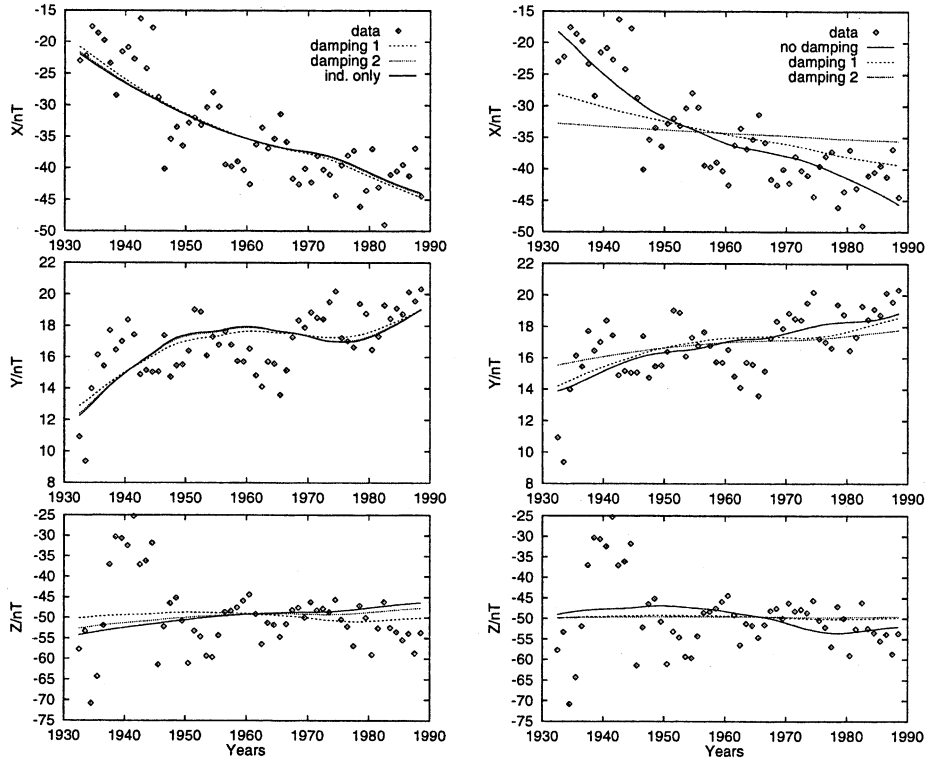

Figure 6. Niemegk: fit to the data when only the remanent field is damped (left) or when only the induced field is damped (right).

time changes accurately. We believe inadequate core–crust separation to be the main source of error in our analysis, and it may be the reason why the model fails to explain the more rapid time variations in the data (*cf.* Fig. 3 for CF3 and Fig. 5 for Lerwick): perhaps some of the core field signal remains in the residuals. Future work should incorporate a fuller model of the crustal field, thereby improving the core field models as well as providing better residuals for the crust.

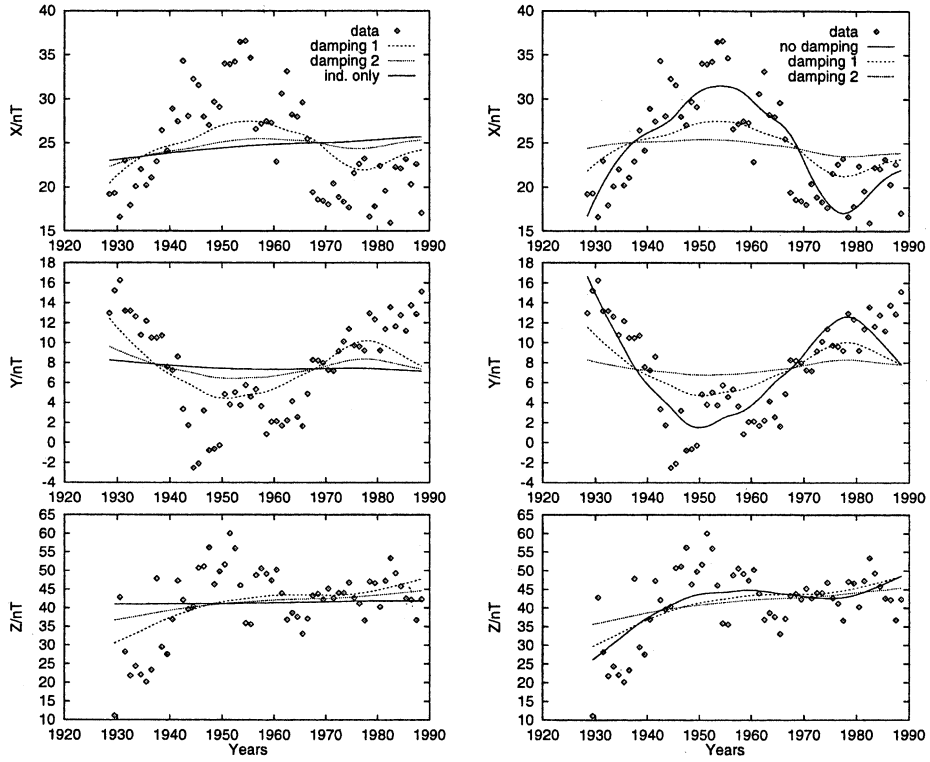

Figure 7. Lovo: fit to the data when only the remanent field is damped (left) or when only the induced field is damped (right).

We have failed to obtain a satisfactory separation between induced and remanent parts, but we have made a convincing case for substantial induced magnetization around almost all the good observatories. Separation of induced and remanent parts requires knowledge of the secular variation for at least two epochs, or knowledge of the main field for at least three epochs if time differentiation is done by differencing. The accuracy of the separation, or resolution, is determined by the volume swept out by the main field between epochs. If this volume is too small it becomes impossible to distinguish between remanence and an induced field with a nearly constant inducing field. The volume is necessarily small because the observation time is short compared with that of secular variation. This is why we have been unable to obtain a satisfactory separation of remanent and induced parts.

It is interesting to compare this study with those of Goldstein & Ward (1966) and Clark *et al.* (1998), who used micropulsations as a source of time variations in the inducing field to detect small magnetic bodies that could be treated as point sources. Their method must also be limited by the small change in the inducing field, which is fundamental to the method, but with modern vector gradiometers it is possible to measure field changes much more accurately than is possible in an observatory running for several decades. Furthermore, the susceptibility is likely to be small near an observatory because they are sited, where possible, in magnetically quiet places. For this reason, the effective volume required for the integrals (1) is likely to be larger than in a typical exploration situation, where one has nearby compact sources.

ACKNOWLEDGMENTS

This work was supported by NERC grant GR3/R9510.

REFERENCES

Barraclough, D.R. & Malin, S.R.C., 1968. Synthesis of international geomagnetic reference field values, *NERC Inst. Geol. Sci.,* **Rept 71/1**, HMSO, London.

Blakely, R.J., 1995. *Potential Theory in Gravity and Magnetic Applications,* Cambridge University Press, Cambridge.

Bloxham, J. & Jackson, A., 1992. Time-dependent mapping of the magnetic field at the core-mantle boundary, *J. geophys. Res.,* **97,** 19 537–19 563.

Bloxham, J., Gubbins, D. & Jackson, A., 1989. Geomagnetic secular variation, *Phil. Trans. R. Soc. Lond.,* **329,** 415–415.

Clark, D.A., Schmidt, P.W., Coward, D.A. & Huddleston, M.P., 1998. Remote determination of magnetic properties and improved drill targeting of magnetic anomaly sources by differential vector magnetometry (DVM), *Expl. Geophys.,* **29,** 312–312.

Craven, D. & Wahba, G., 1979. Smoothing noisy data with spline functions: estimating the correct degree of smoothing by the method of cross-validation, *Numer. Math.,* **31,** 377–377.

Goldstein, N.E. & Ward, S.H., 1966. The separation of remanent from induced magnetism in situ, *Geophysics,* **31,** 779–779.

Menke, W., 1989. *Geophysical Data Analysis: Discrete Inverse Theory,* Academic Press, London.

Sabaka, T.J., Langel, R.A., Baldwin, R.T. & Conrad, J.A., 1997. The geomagnetic field 1900–1995, *J. Geomag. Geoelectr.,* **49,** 157–157.

Shure, L., Parker, R.L. & Backus, G.E., 1982. Harmonic splines for geomagnetic modelling, *Phys. Earth. planet. Inter.,* **28,** 215–215.